UDC 629.7.036.54

A. Tsaritsynskyi,
T. Ahmadi,
T. Nabokina, cand. of tech. sciences

DEVELOPMENT OF GIMBAL
FOR LOW-THRUST LIQUID PROPELLANT ROCKET ENGINE

Overview

Controlling the flight path and the attitude of a rocket-propelled vehicle makes it possible to reach a precise flight destination. Many different mechanisms have been used successfully. In the gimbal scheme, the whole engine is pivoted on a bearing and thus the thrust vector changes its direction.

For small angles (up to 12°) this scheme has negligible losses in specific impulse and is used in many vehicles. It requires a flexible set of propellant piping to allow the propellant to flow from the tanks of the vehicle to the movable engine [1].

Figure 1 and 2 show heavy gimbals of F-1 engine for Saturn V launch vehicle and Space Shuttle Main Engine (SSME). The "seat", "body" and "block" are three parts that turn against each other. The block can turn around the shaft in X axis. The body can turn around the block in the Y axis. The Z axis remains fixed, as the block can't turn 'across' the shaft, and the flat areas on its sides prevent body turning around the block.
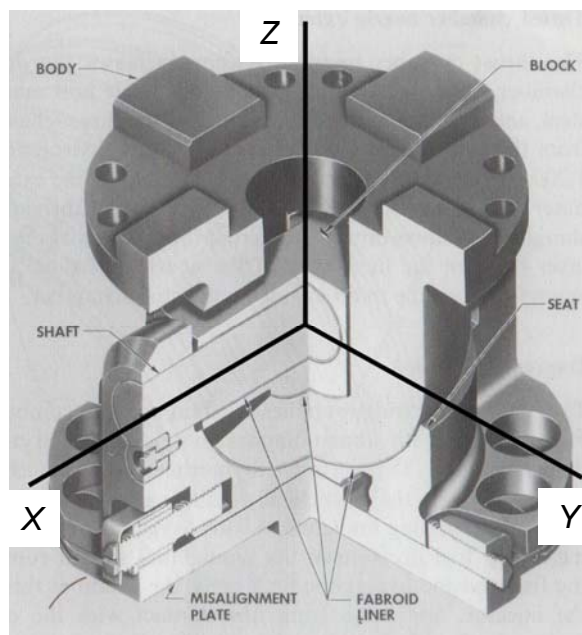

Figure 1 – The gimbal F-1 engine for Saturn V launch vehicle [2]

The highest load is compression load along the Z axis, as the engine fires. Thus the bottom surface of the block pressing against the seat, transferring the largest load. The opposite – tensile load, as the engine hangs before ignition on the bottom of the rocket, is transferred through the interface between the block bottom surface and body inner spherical surface, then from the block to the shaft. X and Y translation is less of a concern, but still the seat-block interface prevents it - transforming it into a much weaker tensile load, that is either prevented by the shaft-block assembly, or completely negated by thrust of the engine exerting a compressive load.
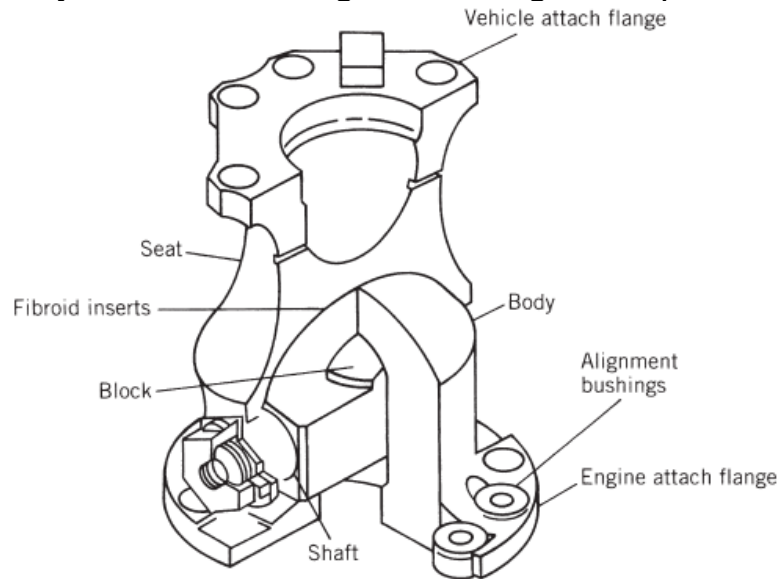

Figure 2 – The gimbal F-1 engine for SSME [3]

Some of the design features and performance requirements of SSME gimbal are listed in Table 1. The maximum angular motion is actually larger than the deflection angle during operation so as to allow for various tolerances and alignments. The actual deflections, alignment tolerances, friction coefficients, angular speeds, and accelerations during operation are usually much smaller than the maximum values listed in the table.

Table 1 – Some requirements of the SSME gimbal [1]

Engine weight to be supported, lbf	~ 7000
Thrust to be transmitted, lbf	512,000
Gimbal assembly weight, lbf	105
Material is titanium alloy	6Al-6V-2Sn
Dimensions (approximate), in.	11 dia. × 14
Maximum operational angular motion, deg	±10.5
Maximum angular capability, deg	±12.5
Angular acceleration (max.), rad/s^2	30
Angular velocity (max.), deg/s	20
Angular velocity (min.), deg/s	10

The alternative structure for gimbal of upper-stage engine for Ariane 5 launch vehicle is shown on Figure 3.

a   b

Figure 4 – Gimbal of upper-stage engine for Ariane 5 launch vehicle:
a – 3D-model; b – prototype with uncovered bearings

The gimbal consists of an engine-side bracket, the gimbal cross, and the stage-side bracket, connected by two pairs of bearings. The distance between the gimbal interface plates amounts to 150 mm.

At an early stage of the development, the decision for rolling bearings was made due to the low friction torque and the low wear of rolling bearings. The decision for a needle roller bearing (Figure 4) was driven by the load capability of the bearing at a given envelope restriction. Four single-row needle roller bearings allow gimbal motion about two axes.

The bracket consists of a circular bore in housing that has varying stiffness along its circumference (Figure 5).

Figure 4 – Single-row needle roller bearing

Figure 5 – Bracket

This type of gimbal will be further designed for the engine developed is previous chapters.

Engine characteristics and gimbal appearance

Main performance characteristics of the engine designed are adduced in Table 2. General view of the engine is shown on Figure 6.

Table 2 – Main performance characteristics of the engine

Parameter	Value
Maximum operational angle, *deg*	±10
Thrust, *N*	2000
Pressure inside the combustion chamber, *MPa*	2
Pressure inside the component-mixing chamber, *MPa*	3

Main parts of gimbal proposed are shown on Figure 7. It incorporates upper and lower brackets, cross-shaft, four bearings, four coverings and eight screws.
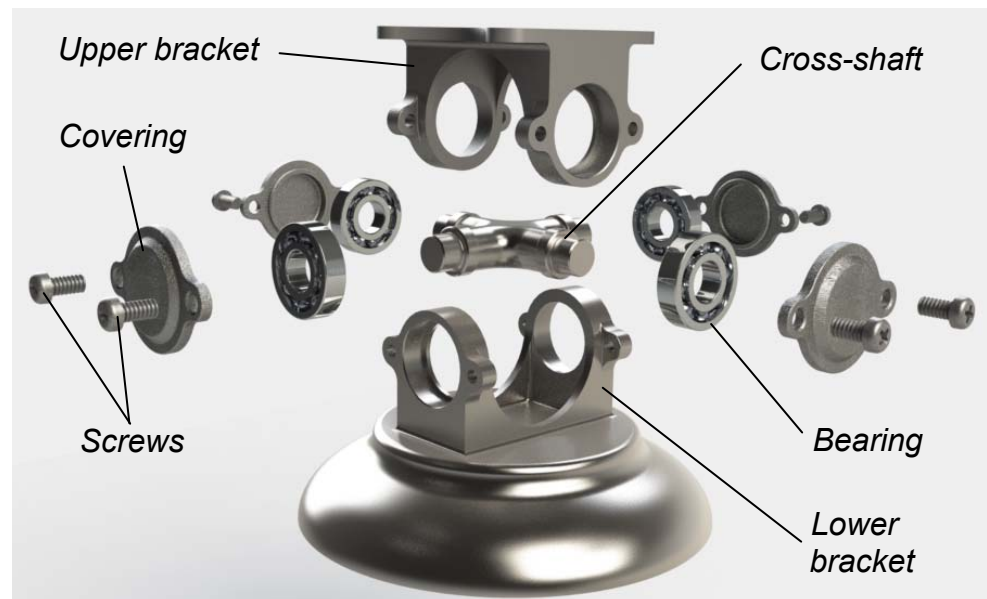
Ø155

435

Figure 6 – View of the engine

Figure 7 – Gimbal assembly (exploded view)

Bearing selection

According to the gimbal type selected, the cross-shaft transfers loads between the brackets through two pair of bearings (Figure 8). The information and recommendations on proper bearing selection are taken from [4].

Due to relatively low thrust of the engine developed (*P* = 2000*N,* see Table 2) the ball bearing type was chosen. In the forward design the safety factor f=1.5 is used. Thus the force *T* transferred through the gimbal will be

$$T = f \cdot P = 1.5 \cdot 2000 = 3000N$$

The loaded ball bearing is capable to withstand radial F_r and axial F_a forces (Figure 9). Taking into account small angles of chamber rotation ($\alpha_{max} = 10°$, see Table 2) the static carrying capacity of the bearing has to be considered. The maximum allowable axial force must be less than 70% of unused static carrying capacity.
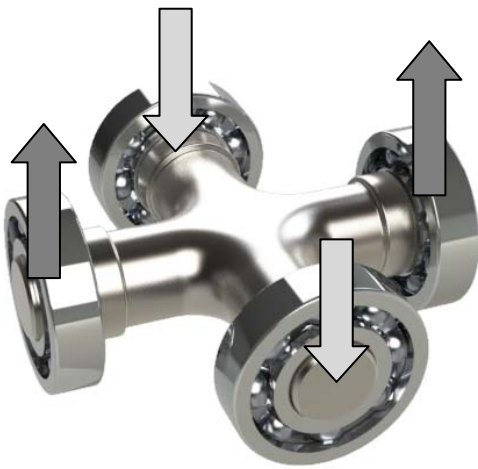
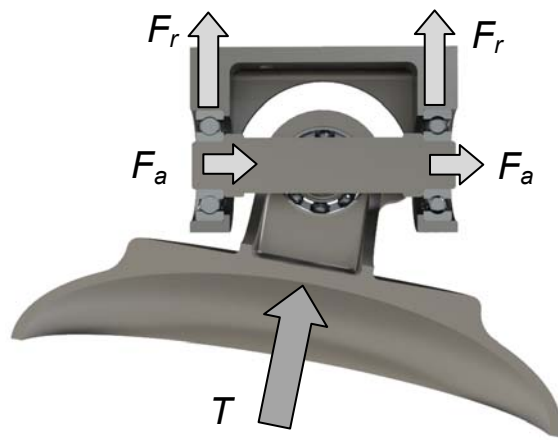Figure 8 – Force transfer through bearings (exploded view)

Figure 9 – Nature of axial and radial loads in bearings of gimbal (section view)

Let's calculate the values of radial F_r and axial F_a forces respectively with α_{max}:

$$F_r = \frac{T}{2} \cdot cos\alpha_{max} = \frac{3000}{2} \cdot cos10° = 1477N;$$

$$F_a = \frac{T}{2} \cdot sin\alpha_{max} = \frac{3000}{2} \cdot sin10° = 260.5N.$$

Main characteristics of ball bearing chosen are given in Table 3.

Table 3 – Characteristics of ball bearing

Bearing Index	Inner diameter, mm	Outer diameter, mm	Width, mm	Static load-bearing capacity, N
7000101	12	28	7	2270

The unused load carrying capacity ΔC

$$\Delta C = C_0 - F_r = 2270 - 1477 = 793 N.$$

The relation δ between of axial force and unused load carrying capacity (taking account the fact that one bearing carries double axial load)

$$\delta = \frac{2 \cdot F_a}{\Delta C} 100\% = \frac{2 \cdot 260.5}{793} 100\% = 65.6\%,$$

which is less than maximum allowable of 70%. The selected bearing meets load requirements.

Finite element analysis of gimbal

The finite element analysis of gimbal assembly is based on full 3D-model of the engine [6, 7] and incorporates two brackets, cross-shaft and the top bottom of the combustion chamber (Figure 10).

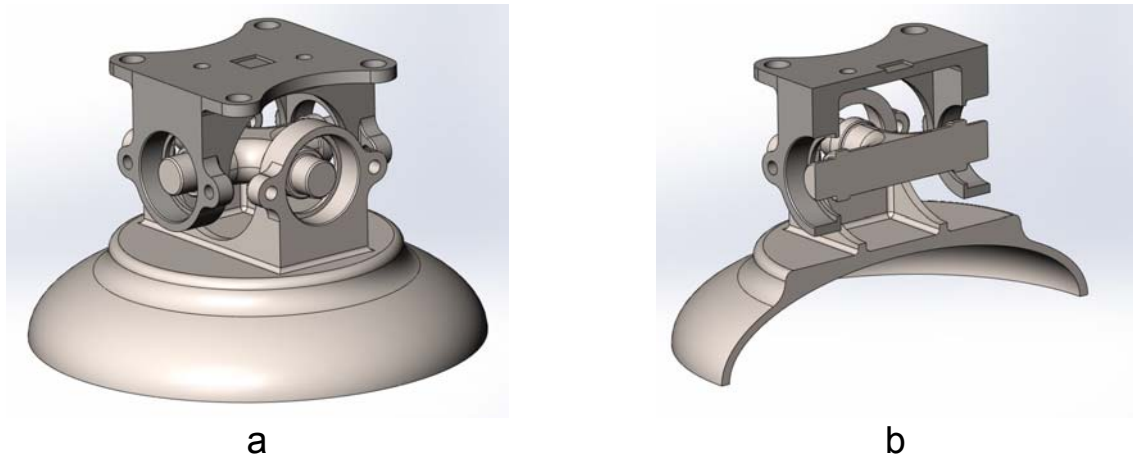a   b

Figure 10 – Geometric model of gimbal assembly for analysis:
a – general view; b – section view

When the engine fires, the gimbal assembly is being loaded by compressive forces caused by thrust. The model is rigidly fixed by the bottom ring surface (Figure 11, a) and also stabilized from accident rotation by adding the slider boundary condition on the auxiliary geometry feature (Figure 11, b).

Bearings are suppressed from the assembly because their analysis is highly non-linear contact problem. Built-in Bearing connector feature is used to bound cross-shaft and brackets thus simulating the stiffness of excluded bearings.

The engine is capable to change its angular position, which can be fully defined by two angles α_1 and α_2, each angle measures between the launch vehicle axis and the chamber axis in planes of control actuators).
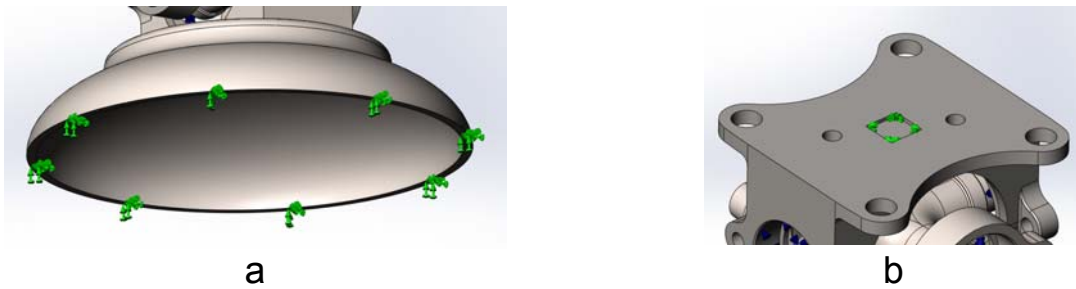
Figure 11 – Displacement constraints:
a – rigid fixation on top bottom; b – slider on upper bracket

Load boundary conditions include:
1) internal pressure in component-mixing chamber (Figure 12, a);
2) reaction force which is taken equal to $T=3000N$ for three cases:

    a) $\alpha_1 = 0$, $\alpha_2 = 0$ (the chamber is in neutral position, Figure 12, b);

    b) $\alpha_1 = \alpha_{max}$, $\alpha_2 = 0$ (Figure 12, c);

    c) $\alpha_1 = \alpha_{max}$, $\alpha_2 = \alpha_{max}$ (Figure 12, d).
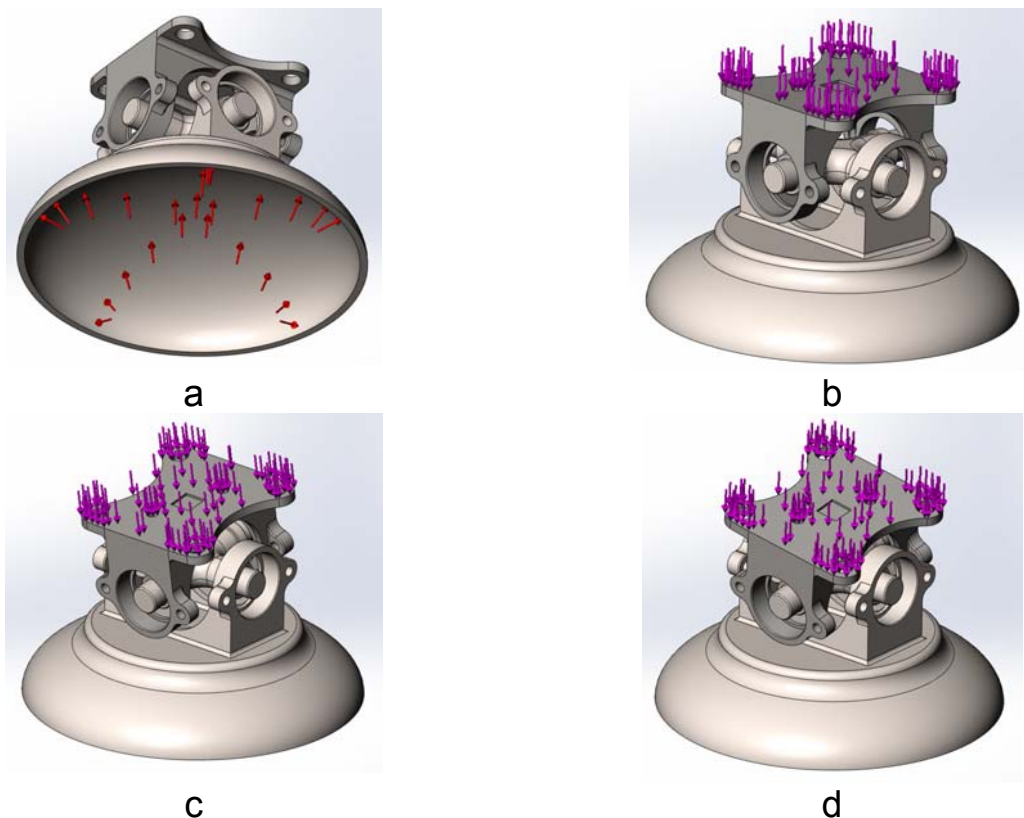

Figure 12 – Load boundary conditions:
a – internal pressure in component-mixing chamber;
b – reaction force ($\alpha_1 = 0$, $\alpha_2 = 0$); c – reaction force ($\alpha_1 = \alpha_{max}$, $\alpha_2 = 0$);
d – reaction force ($\alpha_1 = \alpha_{max}$; $\alpha_2 = \alpha_{max}$)

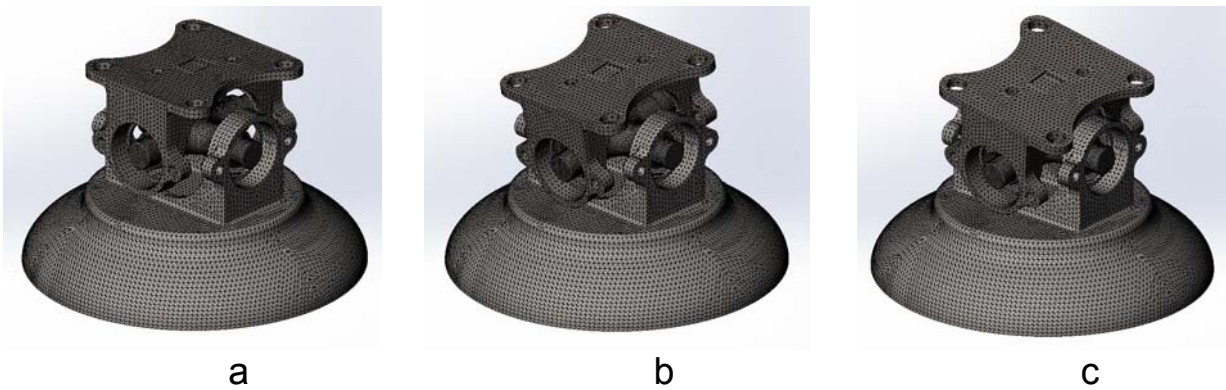Finite element meshes of models are shown on Figure 13.

<div align="center">a   b   c</div>

Figure 13 – Finite element mesh:

$$a - \alpha_1 = 0, \ \alpha_2 = 0; \ b - \alpha_1 = \alpha_{max}, \ \alpha_2 = 0; \ c - \alpha_1 = \alpha_{max}, \ \alpha_2 = \alpha_{max}$$

After calculation is complete, the results can be evaluated. Figure 14 shows the distribution of total displacement in the entire model. The maximum displacement is less than 0.05mm, so the structure is considered to be rigid.
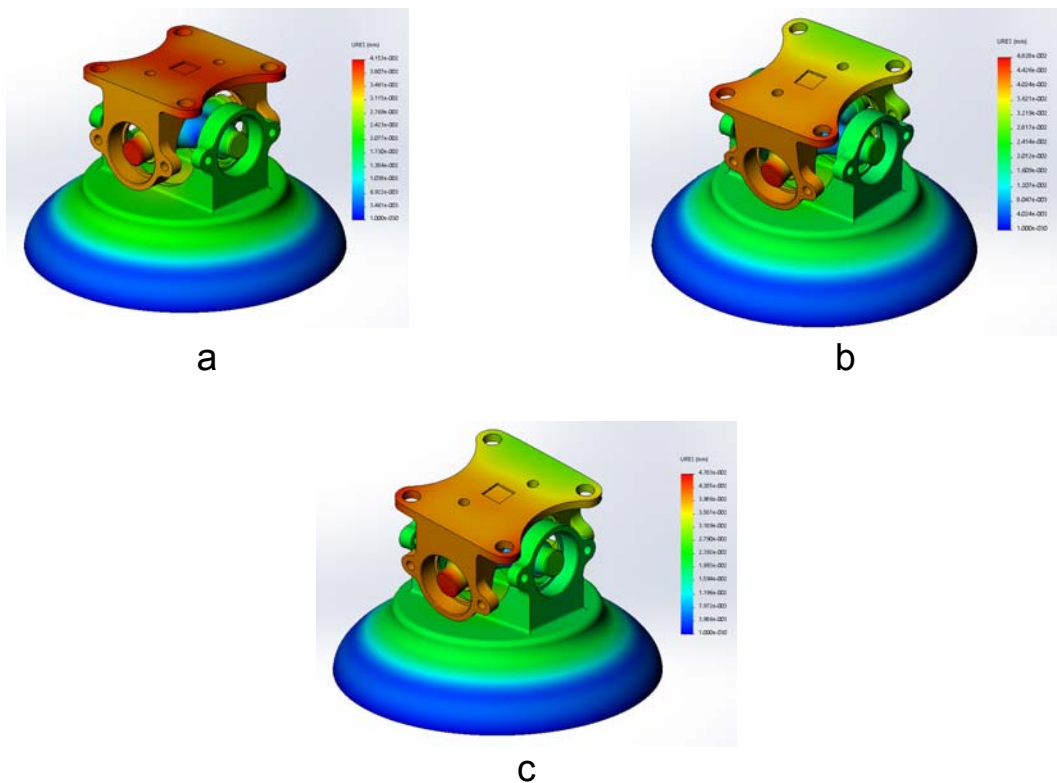

<div align="center">a   b</div>

<div align="center">c</div>

Figure 14 – Total displacements in the entire model (deformation scale – 50):

$$a - \alpha_1 = 0, \ \alpha_2 = 0; \ b - \alpha_1 = \alpha_{max}, \ \alpha_2 = 0; \ c - \alpha_1 = \alpha_{max}, \ \alpha_2 = \alpha_{max}$$

Figures 15 – 17 show stress distribution in every component of the assembly.
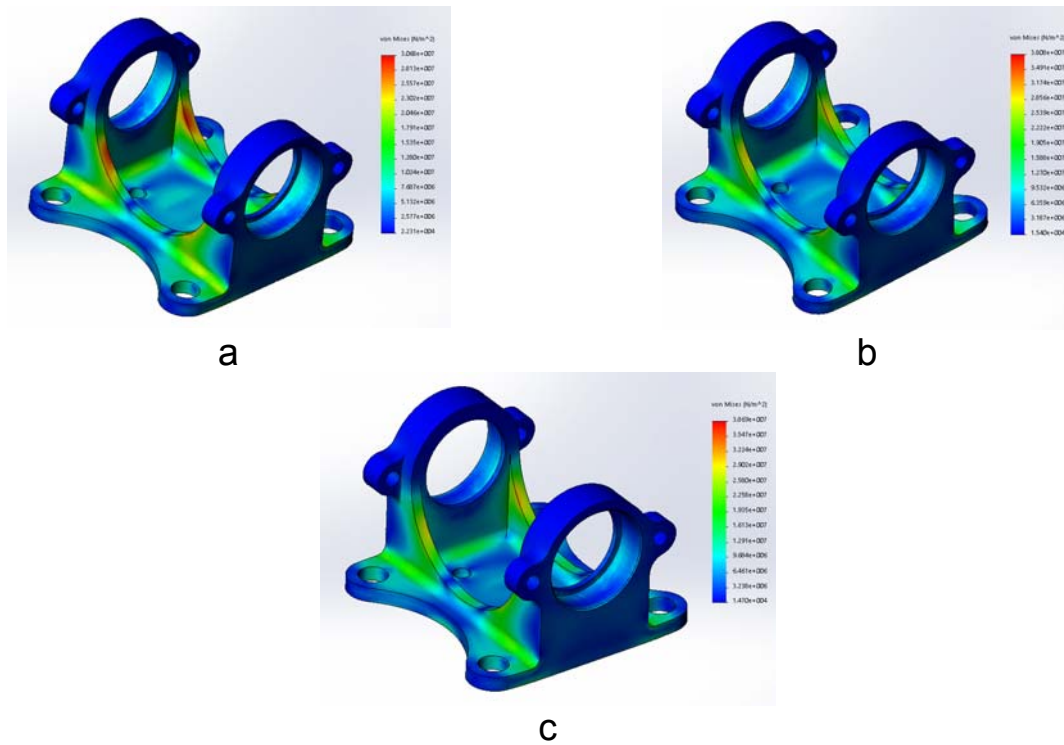

a

b

c

Figure 15 – Von Mises stresses in the upper bracket (deformation scale – 50):
a – $\alpha_1 = 0$, $\alpha_2 = 0$; b – $\alpha_1 = \alpha_{max}$, $\alpha_2 = 0$; c – $\alpha_1 = \alpha_{max}$, $\alpha_2 = \alpha_{max}$
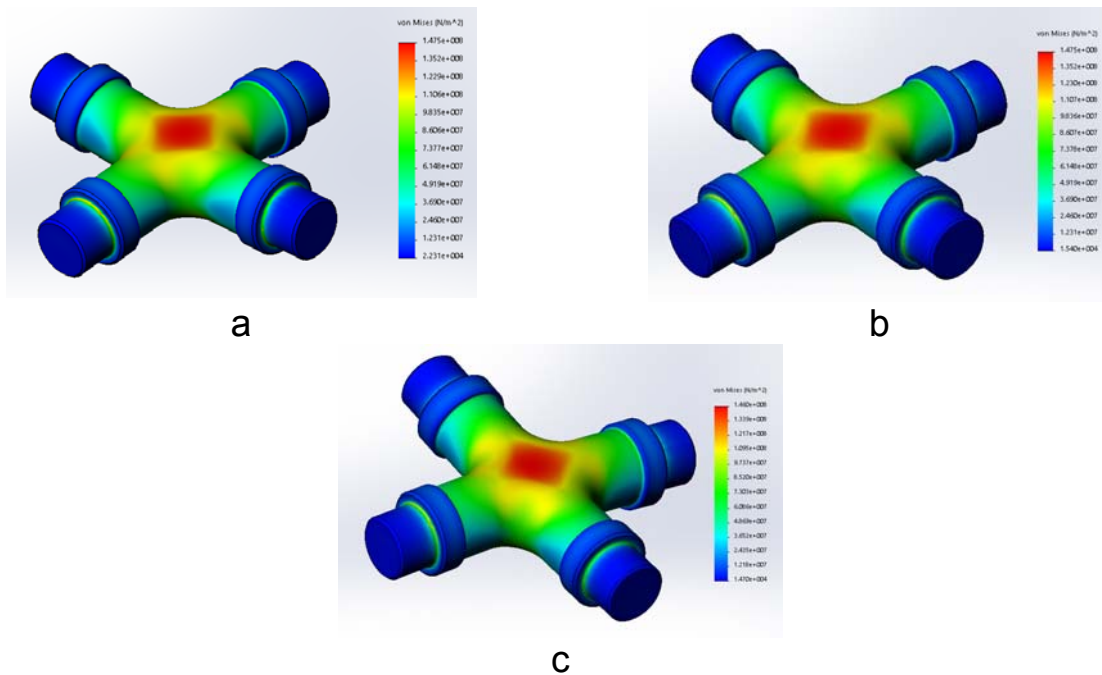

a

b

c

Figure 16 – Von Mises stresses in the cross-shaft (deformation scale – 50):
a – $\alpha_1 = 0$, $\alpha_2 = 0$; b – $\alpha_1 = \alpha_{max}$, $\alpha_2 = 0$; c – $\alpha_1 = \propto_{max}$, $\alpha_2 = \alpha_{max}$
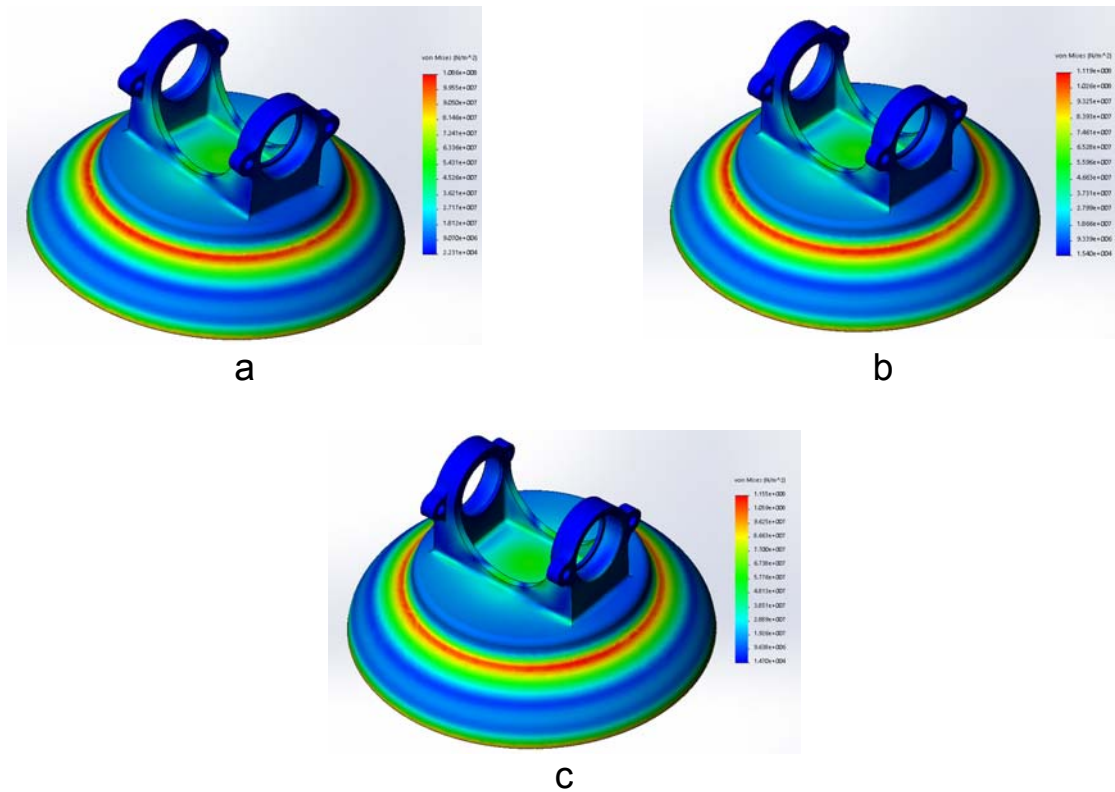
a

b

c

Figure 17 – Von Mises stresses in the lower bracket (deformation scale – 50):
a – $\alpha_1 = 0$, $\alpha_2 = 0$; b – $\alpha_1 = \alpha_{max}$, $\alpha_2 = 0$; c – $\alpha_1 = \alpha_{max}$, $\alpha_2 = \alpha_{max}$

Equivalent stresses in each component do not exceed the elastic zone providing structure integrity during its operation: for upper and lower bracket (steel ЭИ654, $\sigma_{0.2} \approx 350$MPa) maximum von Mises stress is less than 116MPa, for the cross-shaft (steel 30ХГСА, $\sigma_{0.2} \approx 500$MPa) – 148MPa.

It is also important to estimate the angular displacement on the ends because of the axis misalignment requirements for ball bearings: it has to be less than 0.5° [5]. Unfortunately, within a CAE-software used it is not possible to show angular displacements for solid model analysis, but the calculation can be conducted using linear displacements.

Figure 18 shows that the stress-strain state of the cross-shaft do not depends on angles α_1 and α_2, so that it is enough to consider only one load case with $\alpha_1 = \alpha_2 = 0$, where the displacements can be evaluated directly (Figure 19).

Assuming linear law of displacement distribution, we can write a relation

$$tg\Theta = \frac{UZ}{r},$$

where Θ – deflection angle of the end; UZ – longitudinal displacement of the most distant point of cross-section (normal to the cross-section itself), mm; r – distance between neutral plane and the point where the UZ occurs, mm.
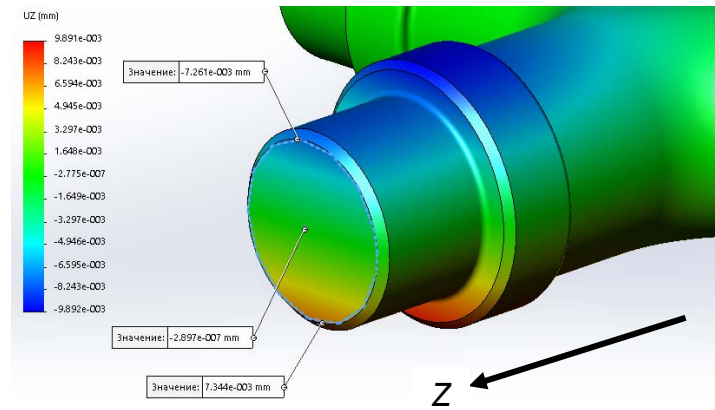
Figure 18 – Axial displacements for deflection angle calculation

Taking *r* = 5.5mm, we can calculate the angle of end section deflection

$$\Theta = arctg\,\frac{UZ}{r} = arctg\,\frac{7.344 \cdot 10^{-3}}{5.5} = 0.0765°,$$

that is smaller than the required limit of $0.5°$.

Conclusion

A variant of gimbal for the low-thrust liquid propellant rocket engine has been developed. Preliminary linear static finite element simulation has proven the design since main structural elements of gimbal meet both strength and stiffness requirements. The gimbal appearance in the engine assembly is shown on Figure 19.
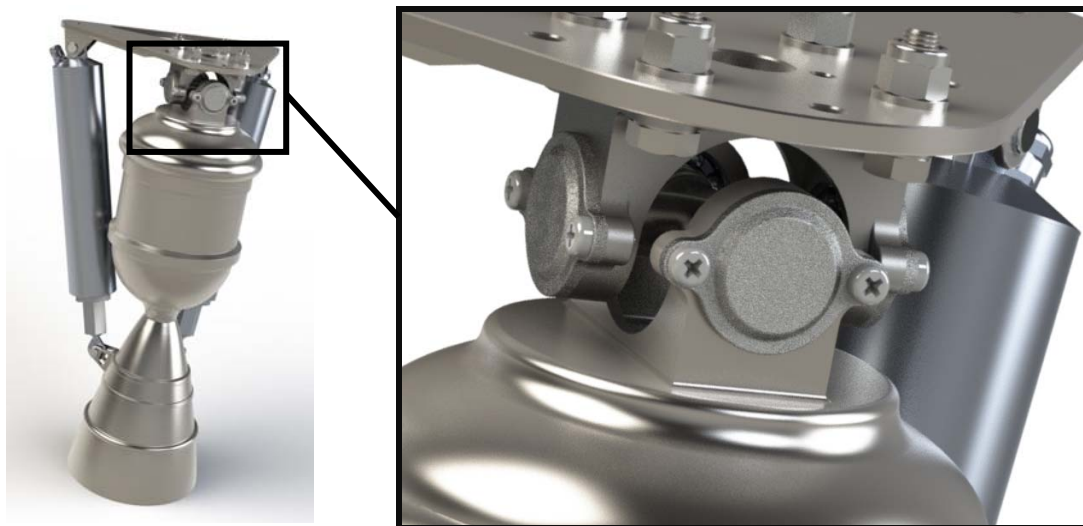

Figure 19 – Gimbal in the engine assembly

At the same time the structure proposed is able to get further optimization of shape and sizes.

List of references

1. Sutton G., Biblarz O. Rocket Propulsion Elements. – 8th ed. – Wiley, 2010. – 786 p.

2. Young A. The Saturn V F-1 Engine. Powering Apollo into History. – New York Springer, 2008. – 324 p.

3. Space Shuttle Main Engine Orientation. Space Transportation System. Training Data. – Boeing, 1998. – 105 p.

4. Neugebauet C., Falkner M., Supper L., Traxler G. Bearing Development for a Rocket Engine Gimbal [Electronic resource] // 38th Aerospace Mechanisms Symposium. – Access mode: http://esmats.eu/amspapers/pastpapers/pdfs/2006/neugebauer.pdf.

5. Перель Л. Я. Подшипники качения. Расчет, проектирование и обслуживание опор: справ. – М. : Машиностроение, 1983. – 543 p.

6. Кондратьев А.В., Кириченко В. В., Царицынский А. А. Проектирование элементов конструкций ракетно-космической техники с использованием конечно-элементной поддержки – Х.: Нац. аэрокосм. ун-т им. Н.Е. Жуковского «Харьков авиац. ин-т», 2018. – 200 с.

7. Кириченко В.В., Кондратьев А.В., Чумак А.А., Царицынский А.А Компьютерные технологии проектирования: учеб. пособие по лаб. практикуму. – Х.: Нац. аэрокосм. ун-т им. Н. Е. Жуковского «Харьк. авиац. ин-т», 2014. – 100 с.